

Institute of Applied Physics, University of Bern, Switzerland

## Passive Microwave Signatures of Landscapes in Winter

C. Mätzler

With 7 Figures

Received March 15, 1993

Revised June 24, 1993

### Summary

The successful application of passive microwave sensors requires signatures for the unambiguous inversion of the remote sensing data. Due to the large number of object types and large variability of physical properties, the inversion of data from land surfaces is a delicate and often ambiguous task. The present paper is a contribution to the assessment of multi-frequency passive microwave signatures of typical objects on land in winter. We discuss the behaviour of measured emissivities at vertical and horizontal polarization over the frequency range of 5 to 100 GHz (incidence angle of 50 degrees) of water and bare soil surfaces, grass and snowcovers under various conditions. These data and their variabilities lead us toward a classification algorithm for some, but not all object classes. Most snowcovers can easily be discriminated from other surfaces, difficulties occur for fresh powder snow if 94 GHz data are not available. The problem of wet snow has found a solution by using a certain combination of observables.

In addition to snowcover types we find large differences between frozen and unfrozen bare soil. On the other hand the different situations of grasscovers show all very similar emissivities.

For the estimation of physical parameters we propose algorithms for certain object classes. The estimation of surface temperature, especially for snow-free land, seems to be feasible, also the estimation of the snow liquid water content at the surface. For estimating soil moisture lower frequencies (e.g. 1.4 GHz) should be used.

For the estimation of the Water Equivalent, WE, we cannot yet find a definitive solution. Certain correlations exist for dry winter snow between WE and observables at frequencies between 10 and 35 GHz. Especially the polarization difference at 10 GHz shows a monotonous increase with increasing WE. Algorithms using higher frequencies

are more sensitive to WE, however they are subject to ambiguities.

### 1. Introduction

The advantages of microwave radiometry for the large-scale observations of climate and hydrologic variables have been stated repeatedly. Impressive results were obtained with data from the Scanning Multichannel Microwave Radiometer (SMMR), especially over the ocean surface (Gloersen et al., 1984; Gloersen and Campbell, 1991) and with the Special Sensor Microwave Imager (SSM/I) as shown by several authors in a special journal issue edited by Hollinger (1990). When it comes to the actual definition of retrieval algorithms for geophysical parameters over land we are faced with the problems of the real world.

I would like to mention the three following problems:

- (1) The surface heterogeneity is of a much smaller scale than the spatial resolution of imaging radiometers. The improved resolutions of future instruments, the European Space Agency's Multichannel Imaging Microwave Radiometer (MIMR) and the Russian scanning IKAR radiometers on Priroda, will partly reduce this problem.
- (2) The emission properties of the earth's surface and the influence of the atmosphere may

change more rapidly than the typical repeat cycle (0.5 to several days) of the observing system.

- (3) The observable – in our case the brightness temperature – may not be sufficiently sensitive to the required geophysical variable (e.g. the snow-water-equivalent). Other variables (e.g. the snow structure) may dominate.

Although the first problem is serious, its effect on parameters used in large-scale models is limited. The successful application of mixed-signature algorithms allows a parametrization of the variables at the given scale of the sensor resolution. This parametrization is required by the hydrologic and climate models anyway. The limitation of mixed-signature algorithms is their inaccuracy to objects at low concentration.

The second problem is more fundamental; it limits the application of multitemporal analysis. Furthermore, the variable influence of the atmosphere hampers the extraction of surface information.

The third problem is the signature problem. Only if we can solve it will be able to construct physical algorithms to retrieve geophysical parameters. If we succeed we will get keys to solve the additional Problems 1 and 2. Therefore this paper will concentrate on the search for passive microwave signatures of land surfaces in winter, spanning the frequency range from 5 to 100 GHz, the range of the future MIMR system.

The original objective was the development of algorithms for snowpack remote sensing. However, since snow is found in different landscapes, we need spectral emissivities of all relevant surface types in order to discriminate snowcover from snow-free land. Therefore, the primary objective must be the development of a signature catalog of all possible surface types, with and without snowcover. The advantage of such a catalog is its potential to define optimized algorithms for each application and adapted to regions of interest. These algorithms will not be limited to snowpack remote sensing, but may include the measurement of surface temperature, including the discrimination between frost and non-frost conditions, vegetation and soil properties.

It is the purpose of this paper to present a status report on a long-term investigation of passive microwave signatures over the frequency range from 5 to 100 GHz. This range covers

the frequencies of SMMR, SSMI, of the future MIMR (Menard and Thornbury, 1989) and IKAR (Armand and Kutuza, 1993). The results of experiments made with the multi-frequency radiometer system PAMIR at two test sites in Switzerland will be described. Although the collected data base does not yet cover all possible landscapes (e.g. forest signatures are missing) the experimental dataset already provides a valuable contribution to the spectral and polarimetric signatures of land surfaces. According to the authors' knowledge PAMIR has been the only 5-to-100 GHz-radio-meter system for in-situ signature studies of the earth's surface. Therefore the present paper has to focus on data from this system. With the progress in the development of MIMR some new radiometer systems have recently been built (e.g. the French PORTOS, J. P. Wigneron, LERTS, Toulouse, personal communication) or are currently under construction (A. W. England, Univ. of Michigan, Ann Arbor, personal communication). Complementary studies to be made with these systems should be encouraged.

## 2. The Data Base

### 2.1 The PAMIR System

PAMIR is the acronym for "Passive and Active Microwave and Infrared Radiometer". This sensor system consists of five microwave radiometers (Table 1), an X-band scatterometer and a thermal infrared radiometer. The radiometers were built and first operated by Roland Hofer (Schanda and Hofer, 1977) for signature research on alpine snowpacks. These measurements continued until 1987 at the alpine test site, Weissfluhjoch (Mätzler, 1987). Then PAMIR was relocated to the agricultural test site "Tannacker" at Moosseedorf

Table 1. Specifications of the PAMIR Microwave Radiometers

Radiometer Number	1	2	3	4	5
Center Frequency, GHz	4.9	10.4	21	35	94
Bandwidth, GHz	0.2	1.2	0.8	0.8	2.0
Sensitivity, K (at 1s integr. time)	0.1	0.1	0.1	0.1	0.2
Viewing angle	all between nadir and zenith				
Polarization	any linear polarization				
3-dB beam width of horn antenna, deg.	10	9	9	9	9

near Bern (Mätzler, 1990). There, the scatterometer and the infrared radiometer were removed.

## 2.2 PAMIR Data from Weissfluhjoch (SLF)

More than 200 different snow situations were observed with PAMIR at Weissfluhjoch together with several snow-free situations with a rocky (gravel-type) soil surface (Mätzler, 1987). Here we will present a revised version which includes new data, a new definition of object classes, and updated quality assurance of earlier data. The object classes of Weissfluhjoch will be identified by SLF, the German acronym of the Snow and Avalanche Research Station at this test site.

SLF\_BARE represents nine different observations of the snow-free test site in wet and dry, warm and cold conditions (unfrozen only).

SLF\_SHALLOW represents 11 situations of winter snow with water equivalents (WE) between 4 and 10 cm. Winter snow is dry, and it has not undergone melt metamorphism.

SLF\_MEDIUM represents 12 situations of winter snow with WE between 10 and 25 cm.

SLF\_DEEP represents 50 situations of deep winter snow with WE between 25 and 63 cm.

SLF\_WET represents 53 situations of wet snow (at least a wet surface layer).

SLF\_THINCRUST represents 20 situations of wet snow covered by refrozen crust whose thickness is between 1 and 3 cm. (In earlier work these data were included in wet snow).

SLF\_THICKCRUST represents 15 situations of wet snow covered by a 4 to 30 cm thick layer of refrozen snow.

SLF\_BOTTOMCRUST represents 6 situations of a special snow situation which was observed in late 1984 and early 1985. An abundant snow fall in autumn 1984 metamorphosed to a 40 cm thick, hard crust and formed the bottom of the new winter snowcover. The crust was frozen to the ground in contrast to the other crusts. In areas of important temperature variations in winter such crusts can occur quite often, and because their emissivities are different from the other snow covers we included them as a special class. In addition, the bottom crust is similar to frozen firn; therefore, we expect similar signatures for temperate glaciers in winter. The bottom crust of 1984–1985 was more strongly stratified than the refrozen surface crusts. So there is a distinct difference in polarization.

The word “crust” also implies that extended periods (several days) of wet snow with melt metamorphism preceded the crust formation. The density is about  $0.4 \text{ g/cm}^3$  or higher, and the grains are quasi spherical with diameters of about 1 mm.

## 2.3 PAMIR Data from Moosseedorf

The observations reported here were made between October and April of the years 1989 to 1993 on bare soil and grass at different conditions, and sometimes covered with snow. (For a catalog of the entire dataset, see Mätzler, 1992a).

The following object classes were identified:

BARE\_SOIL represents 9 situations of bare sandy loam soil at temperatures between 0 and  $25^\circ\text{C}$ , volumetric soil moistures between 12% and 45%.

FROZEN\_SOIL represents two situations of frozen bare soil with surface temperatures of  $-6^\circ\text{C}$  and  $-1^\circ\text{C}$ , respectively, mostly frozen soil moisture of about 40% by volume.

SHORT\_GRASS represents 9 situations with grass cover, height 5–10 cm, volumetric soil moisture 13% to 60%, grass temperature above  $-1^\circ\text{C}$ .

MEDIUM\_GRASS represents 4 situations of grass cover with height between 15 and 32 cm, and temperatures  $T > 0^\circ\text{C}$ .

FROST\_GRASS represents 3 situations of short grass with hoar frost at temperatures between  $-2^\circ\text{C}$  and  $-5^\circ\text{C}$ .

FROZEN\_GRASS represents 4 situations of short grass without hoar frost at temperatures between  $-1.7^\circ\text{C}$  and  $-5^\circ\text{C}$ , soil at  $0^\circ\text{C}$  to  $-2^\circ\text{C}$ .

GRASS\_AFTER\_SNOW represents 2 different situations measured just after snowmelt, when the short grass cover was flat on the ground.

POWDER represents 4 situations of 24 to 37 cm deep powder snow at temperatures between  $-3^\circ\text{C}$  and  $-13^\circ\text{C}$ , with WE near 4 cm. The grass-covered soil was first frozen and later unfrozen. Most of this dry snow was 1 to 7 days old.

BOTTOMCRUST represents 2 situations of aged, refrozen snow (depths of 6 and 15 cm) on frozen ground.

CRUST is one situation of 10 cm refrozen snow on top of 3 cm of wet snow with unfrozen ground.

The situations with wet snow are not included here, because they are similar to the ones at Weissfluhjoch.

Most snow situations were measured in the winter season 1990 to 1991 with the same short grass cover whose water content was near 0.4 kg/m<sup>2</sup>. We considered the grass to be unfrozen at temperatures higher than -1 °C (due to its salinity). However, the freezing temperature of the soil was very close to 0 °C as shown by the soil dielectric data (at 600 MHz) and by the soil hardness. The real part of the dielectric permittivity of frozen soil was between 4.8 and 5.4 whereas for unfrozen soil in winter the observed values were usually larger than 20 (Mätzler, 1992a).

## 2.4 Emissivities of Object Classes

In order to separate atmospheric effects from snow signatures we transformed the in-situ observed brightness temperatures,  $T_p$  (polarization  $p = v, h$ ), to emissivities,  $e_p$ , or reflectivities,  $r_p$ , respectively, according to

$$e_p = 1 - r_p = \frac{T_p - T_s}{T - T_s}; \quad p = h, v \quad (1)$$

where  $T$  is the effective object temperature and  $T_s$  is the brightness temperature of the sky as observed near the surface in the relevant direction. For a specularly reflecting surface the zenith angle of this direction equals the incidence angle of  $T_p$ , and for a Lambertian surface with an optically thin atmosphere the zenith angle is 60° (Schanda, 1986, p. 150; Mätzler, 1987, p. 306).

Brightness temperatures,  $T_p$ , can easily be computed from emissivities and typical  $T_s$  values using Eq. (1). At the test site, Tannacker, in Moosseedorf the average  $T_s$  at a zenith angle of 60° is 8 K at 4.9 GHz, 11 K at 10.4 GHz, 48 K at 21 GHz, 38 K at 35 GHz, and 98 K at 94 GHz. At the alpine test site the average sky brightness temperatures are somewhat smaller. More details about  $T_s$  at the PAMIR frequencies can be found in Mätzler (1992b).

The object classes described in the previous section were defined on the one hand on the basis of ground-truth criteria, and on the other hand on a simple distribution of emissivities to be described by mean values and standard deviations. This numerical information is presented in Tables 2 and 3. We limit the presentation to a constant incidence angle of 50° measured from the vertical. For the Weissfluhjoch data we averaged measurements made at 45° and 55° to get the values at 50°,

and for the data of Moosseedorf we were often limited to observations at angles of at least 55°. However, since the angular dependence is not very strong, especially in case of grass, we took the values at 55° to represent the ones we wanted at 50°. There is a small uncertainty arising from this offset.

The mean spectral emissivities at the PAMIR frequencies at horizontal ( $e_h$ ) and vertical ( $e_v$ ) polarization are given in Table 2 for each object class. The additional class WATER\_OC-8C represents calculated emissivities of a smooth liquid-water surface. The numbers are averaged values of emissivities at 0 °C and 8 °C. The Fresnel formulae were used together with the Debye Equation for the dielectric permittivity of freshwater (Ulaby et al. 1986, Equations E.14 to E.19).

The standard deviations of emissivities and of simple differences within each class ( $N > 1$ ) are given in Table 3. For WATER, the values are computed differences of emissivities at 8 °C and at 0 °C to indicate a typical temperature variation of lake emissivities. The additional effect of roughness due to waves was neglected.

A graphical presentation of emissivity data of 15 classes from Tables 2 and 3 is given in Fig. 1a–o: These Figures are useful to get a general view of the type of spectra and of their variability. At certain frequencies and polarizations we find highly stable emissivities. These may be used as tie points in inversion algorithms. At other frequencies the variability may be large; there the emissivity depends on one or more physical variables (e.g. soil moisture, snow liquid water content, etc.); thus the variability is mostly systematic. For certain linear combinations such as the polarization difference at a given frequency or the spectral difference at a given polarization we may find additional variability or constancy which can be useful for discrimination of objects or for the determination of a certain physical parameter. The only combinations shown in Fig. 1 are the polarization differences. Other combinations can be extracted from Tables 2 and 3.

Figures 1a–c are the three types of bare surfaces where the unfrozen bare soil (Fig. 1a) has the largest variability (standard deviation), especially at the lowest frequency due to variable soil moisture conditions (e.g. Jackson and Schmugge, 1989). Soil moisture was measured in the top 0–3 cm, and the soil dielectric constant in the top

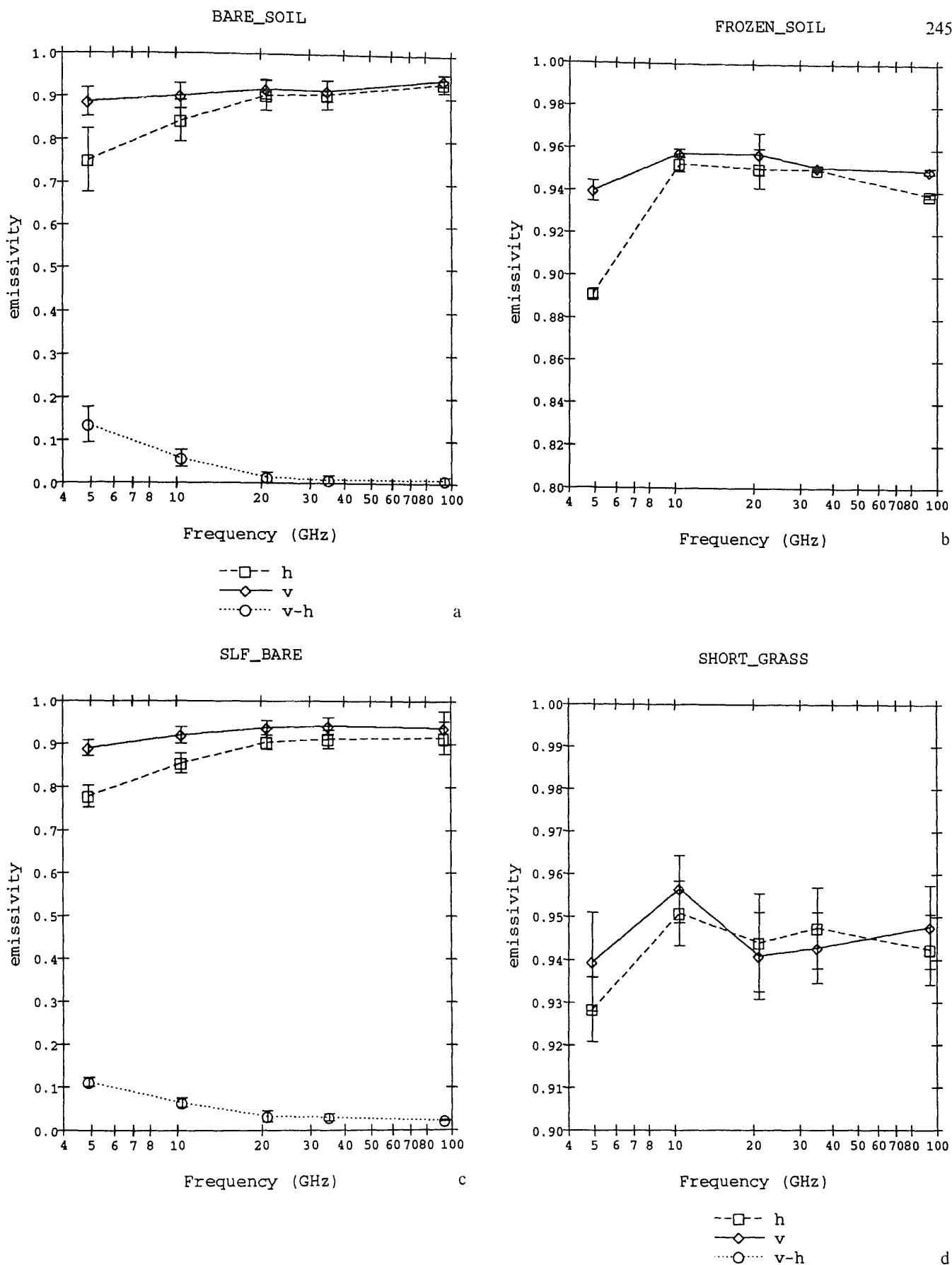


Fig. 1. Measured spectra of emissivities,  $e_v$ ,  $e_h$ , and of  $e_v - e_h$  at  $50^\circ$  off nadir, mean values and standard deviations, of object classes defined in Section 2: (a) BARE\_SOIL; (b) FROZEN\_SOIL; (c) SLF\_BARE; (d) SHORT\_GRASS; (e) MEDIUM\_GRASS; (f) FROST\_GRASS; (g) POWDER snow; (h) SLF\_SHALLOW winter snow; (i) SLF\_MEDIUM winter snow; (j) SLF\_DEEP winter snow; (k) SLF\_WET snow surfaces; (l) SLF\_THINCRUST on wet snow; (m) SLF\_THICKCRUST on wet snow; (n) SLF\_BOTTOMCRUST below winter snow; (o) BOTTOMCRUST at Moosseedorf

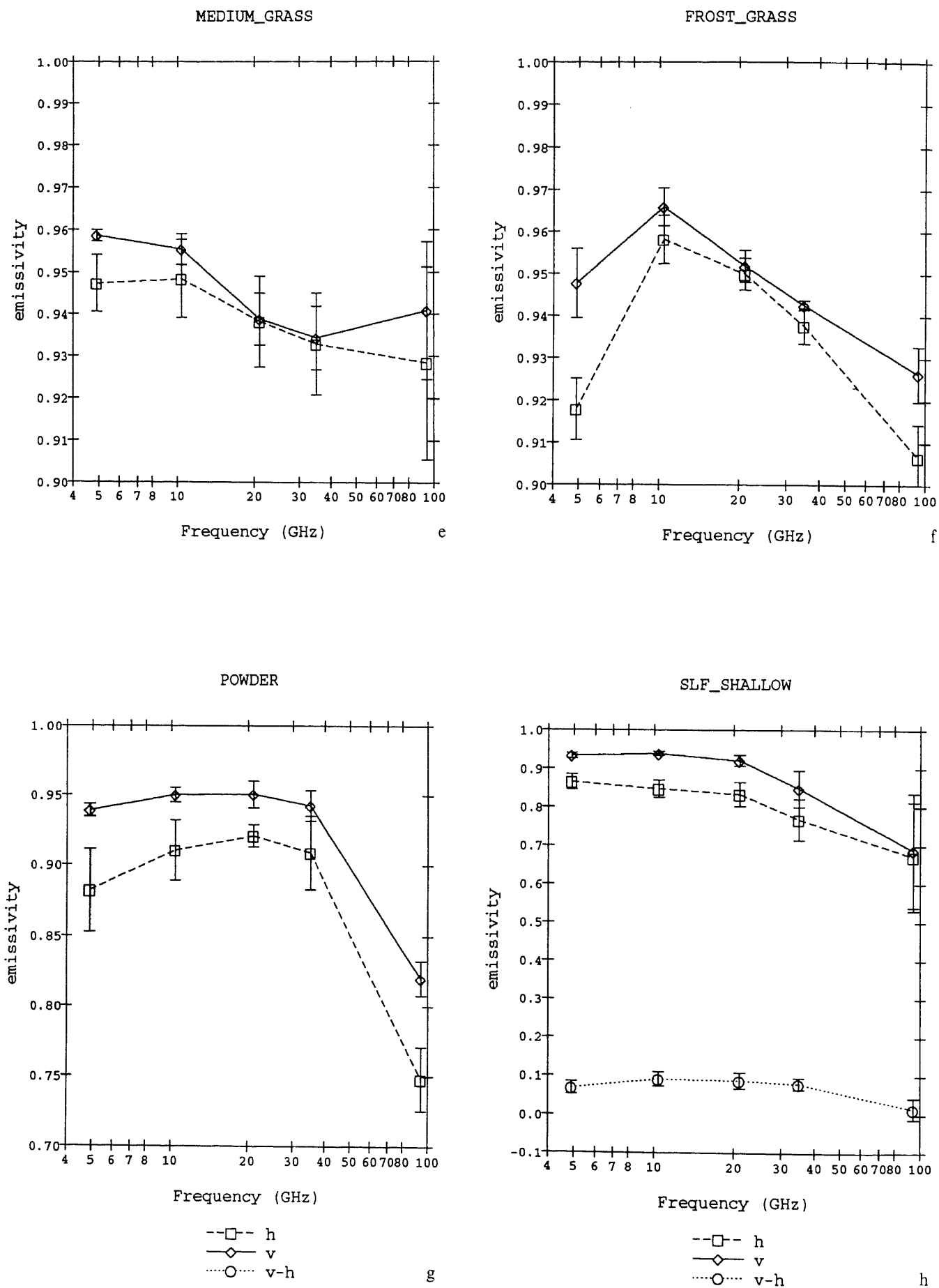


Fig. 1e-h

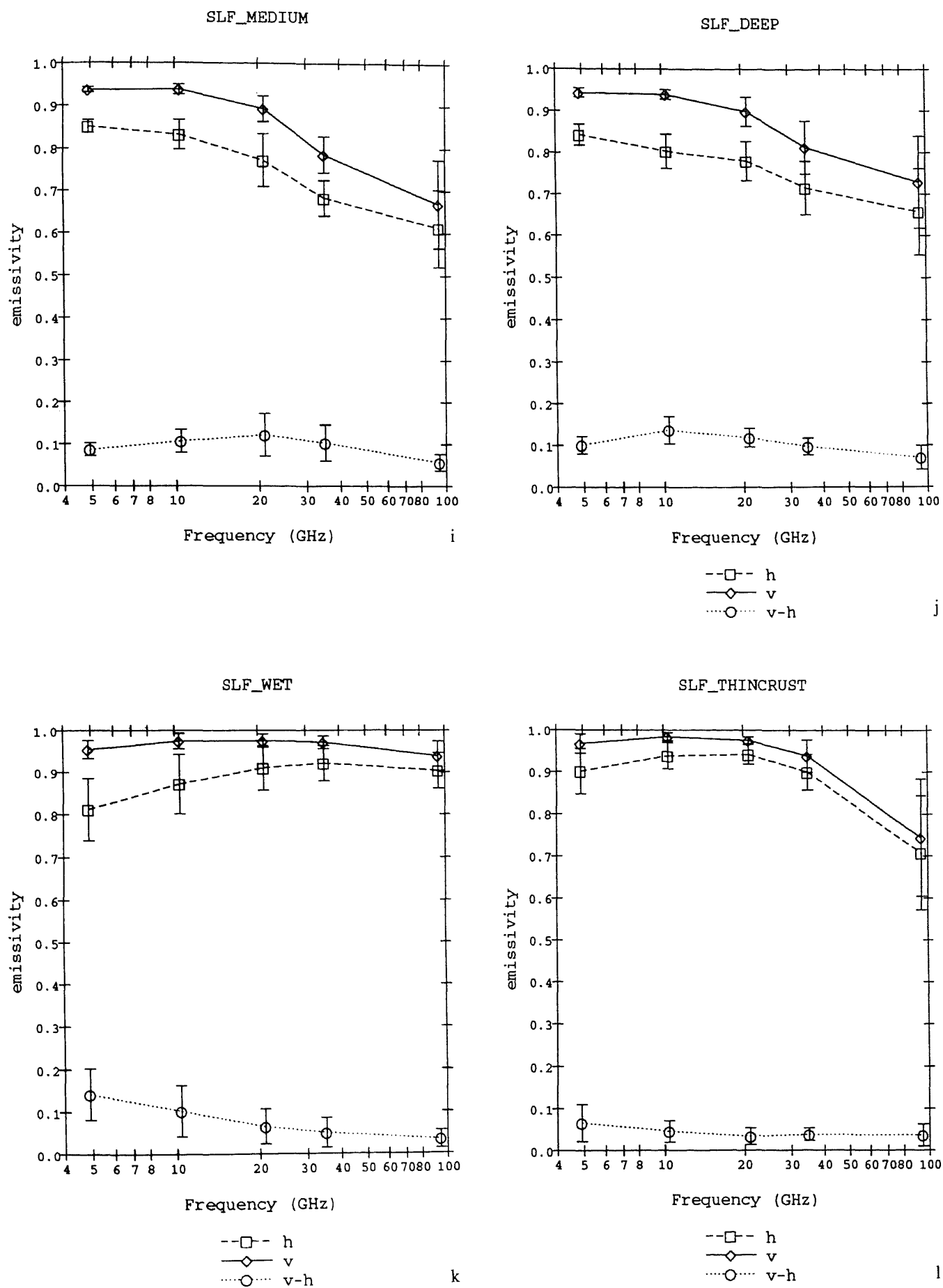


Fig. 1i-l

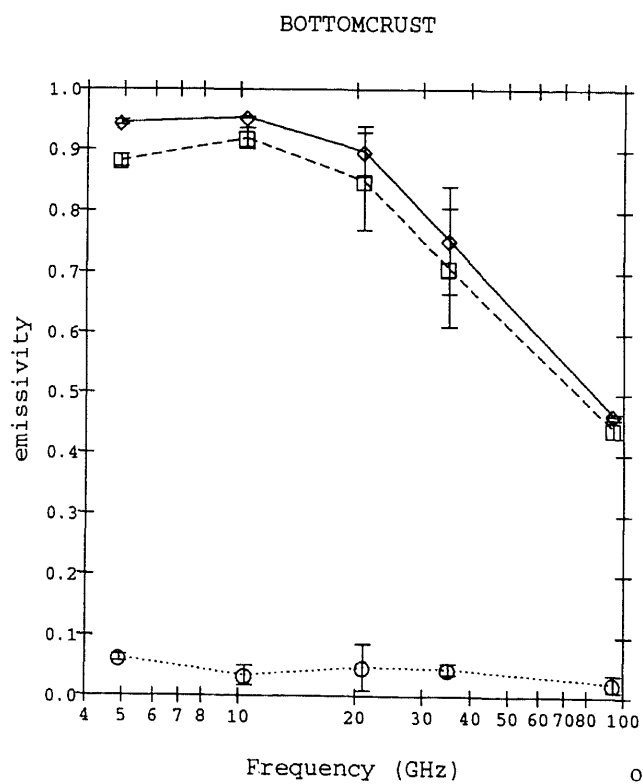
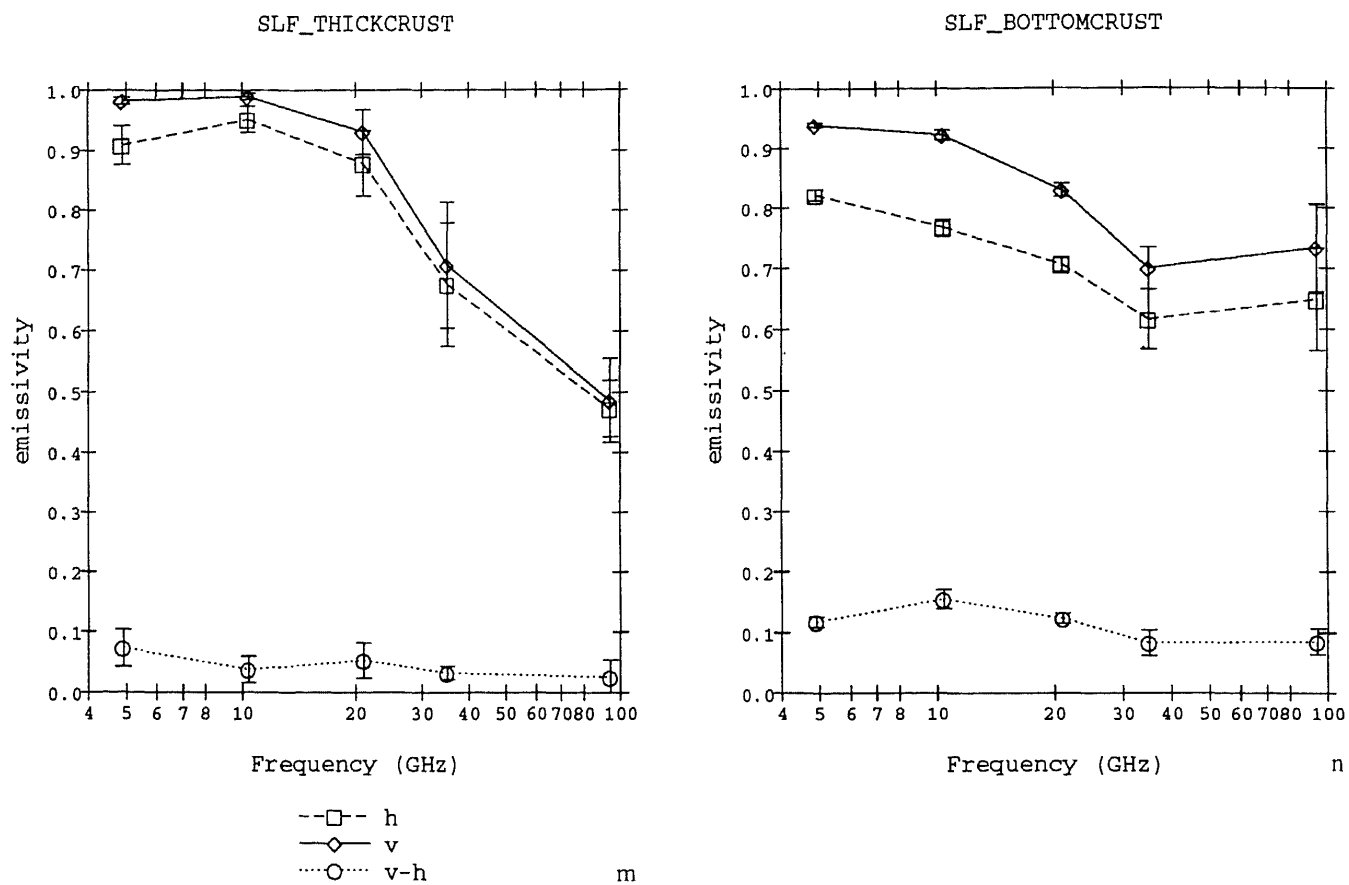


Fig. 1m-o

Table 2. Object Classes, and Mean Values of Emissivities  $e_h$  at Horizontal and  $e_v$  at Vertical Polarization (incidence angle  $50^\circ$ ). The frequency in GHz is given on the top row. Simple differences of emissivities are given in Columns 11 to 23, and a special linear combination (Eq. 2) is shown in the last column

0 Object	1 $e_h$ 4.9	2 $e_h$ 10.4	3 $e_h$ 21	4 $e_h$ 35	5 $e_h$ 94	6 $e_v$ 4.9	7 $e_v$ 10.4	8 $e_v$ 21
1 WATER_0-8C	0.2489	0.2660	0.3062	0.3562	0.5021	0.5002	0.5270	0.5872
2 BARE_SOIL	0.7509	0.8430	0.9035	0.9068	0.9354	0.8868	0.9007	0.9178
3 FROZEN_SOIL	0.8911	0.9528	0.9509	0.9507	0.9384	0.9399	0.9578	0.9577
4 SLF_BARE	0.7780	0.8552	0.9043	0.9111	0.9148	0.8900	0.9203	0.9377
5 SHORT_GRASS	0.9284	0.9508	0.9440	0.9474	0.9424	0.9395	0.9565	0.9409
6 MEDIUM_GRASS	0.9473	0.9484	0.9382	0.9329	0.9284	0.9586	0.9554	0.9388
7 FROZEN_GRASS	0.9188	0.9618	0.9591	0.9553	0.9370	0.9495	0.9674	0.9561
8 FROST_GRASS	0.9178	0.9581	0.9499	0.9375	0.9066	0.9477	0.9658	0.9517
9 GRASS_AFTER_SNOW	0.9018	0.9105	0.9013	0.9016	0.9053	0.9121	0.9246	0.9051
10 SLF_WET	0.8123	0.8726	0.9106	0.9215	0.9039	0.9545	0.9750	0.9756
11 POWDER	0.8819	0.9105	0.9211	0.9091	0.7481	0.9391	0.9503	0.9508
12 SLF_SHALLOW	0.8653	0.8468	0.8330	0.7682	0.6722	0.9340	0.9384	0.9213
13 SLF_MEDIUM	0.8505	0.8315	0.7713	0.6822	0.6121	0.9367	0.9380	0.8929
14 SLF_DEEP	0.8427	0.8030	0.7799	0.7153	0.6576	0.9434	0.9398	0.8985
15 SLF_THINCRUST	0.9015	0.9384	0.9420	0.9004	0.7074	0.9674	0.9843	0.9758
16 SLF_THICKCRUST	0.9095	0.9522	0.8783	0.6768	0.4722	0.9828	0.9897	0.9311
17 SLF_BOTTOMCRUST	0.8218	0.7672	0.7055	0.6155	0.6482	0.9392	0.9220	0.8288
18 BOTTOMCRUST	0.8820	0.9193	0.8495	0.7077	0.4429	0.9446	0.9536	0.8979
19 CRUST	0.8254	0.8155	0.7904	0.7182	0.4809	0.9174	0.9328	0.9172
0 Object	9 $e_v$ 35	10 $e_v$ 94	11 $v-h$ 4.9	12 $v-h$ 10.4	13 $v-h$ 21	14 $v-h$ 35	15 $v-h$ 94	16 $h_{10}-h_5$
1 WATER_0-8C	0.6552	0.8145	0.2512	0.2611	0.2809	0.2989	0.3124	0.0170
2 BARE_SOIL	0.9151	0.9438	0.1359	0.0577	0.0143	0.0083	0.0084	0.0921
3 FROZEN_SOIL	0.9516	0.9501	0.0488	0.0050	0.0067	0.0010	0.0117	0.0617
4 SLF_BARE	0.9419	0.9375	0.1120	0.0651	0.0333	0.0308	0.0227	0.0772
5 SHORT_GRASS	0.9428	0.9477	0.0111	0.0057	-0.0031	-0.0046	0.0052	0.0225
6 MEDIUM_GRASS	0.9343	0.9408	0.0114	0.0070	0.0006	0.0014	0.0124	0.0011
7 FROZEN_GRASS	0.9523	0.9481	0.0307	0.0056	-0.0031	-0.0030	0.0111	0.0429
8 FROST_GRASS	0.9425	0.9263	0.0299	0.0078	0.0019	0.0049	0.0197	0.0402
9 GRASS_AFTER_SNOW	0.9097	0.9200	0.0103	0.0141	0.0038	0.0081	0.0147	0.0087
10 SLF_WET	0.9718	0.9385	0.1423	0.1023	0.0650	0.0502	0.0345	0.0604
11 POWDER	0.9428	0.8201	0.0571	0.0398	0.0297	0.0337	0.0720	0.0286
12 SLF_SHALLOW	0.8483	0.6885	0.0687	0.0915	0.0883	0.0801	0.0163	-0.0185
13 SLF_MEDIUM	0.7850	0.6688	0.0862	0.1065	0.1216	0.1028	0.0566	-0.0190
14 SLF_DEEP	0.8129	0.7283	0.1007	0.1367	0.1186	0.0976	0.0707	-0.0397
15 SLF_THINCRUST	0.9384	0.7438	0.0659	0.0459	0.0337	0.0381	0.0364	0.0369
16 SLF_THICKCRUST	0.7089	0.4859	0.0733	0.0375	0.0527	0.0321	0.0255	0.0427
17 SLF_BOTTOMCRUST	0.6990	0.7333	0.1173	0.1548	0.1233	0.0835	0.0852	-0.0547
18 BOTTOMCRUST	0.7533	0.4663	0.0627	0.0343	0.0483	0.0456	0.0234	0.0373
19 CRUST	0.8095	0.5023	0.0920	0.1174	0.1269	0.0912	0.0214	-0.0099
0 Object	17 $h_{21}-h_{10}$	18 $h_{35}-h_{21}$	19 $h_{94}-h_{35}$	20 $r_{10}-r_5$	21 $r_{21}-r_{10}$	22 $r_{35}-r_{21}$	23 $r_{94}-r_{35}$	24 COMB
1 WATER_0-8C	0.0403	0.0500	0.1459	0.0269	0.0601	0.0680	0.1593	0.4565
2 BARE_SOIL	0.0605	0.0033	0.0286	0.0139	0.0171	-0.0027	0.0286	0.0371
3 FROZEN_SOIL	-0.0019	-0.0003	-0.0122	0.0179	-0.0001	-0.0060	-0.0015	0.0312
4 SLF_BARE	0.0491	0.0068	0.0103	0.0303	0.0173	0.0042	0.0027	0.0646
5 SHORT_GRASS	-0.0068	0.0034	-0.0050	0.0170	-0.0156	0.0019	0.0049	0.0391
6 MEDIUM_GRASS	-0.0102	-0.0053	-0.0044	-0.0033	-0.0166	-0.0045	0.0066	0.0723
7 FROZEN_GRASS	-0.0027	-0.0038	-0.0184	0.0178	-0.0113	-0.0037	-0.0043	0.0447
8 FROST_GRASS	-0.0082	-0.0123	-0.0309	0.0181	-0.0141	-0.0093	-0.0161	0.0847
9 GRASS_AFTER_SNOW	-0.0092	0.0004	0.0037	0.0125	-0.0195	0.0046	0.0103	0.0706
10 SLF_WET	0.0380	0.0109	-0.0062	0.0204	0.0007	-0.0039	-0.0249	0.2272
11 POWDER	0.0105	-0.0119	-0.1610	0.0113	0.0005	-0.0080	-0.1227	0.1257
12 SLF_SHALLOW	-0.0138	-0.0648	-0.1040	0.0044	-0.0171	-0.0730	-0.1703	0.5302
13 SLF_MEDIUM	-0.0602	-0.0892	-0.0725	0.0013	-0.0451	-0.1079	-0.1097	0.7899
14 SLF_DEEP	-0.0232	-0.0646	-0.0400	-0.0036	-0.0413	-0.0856	-0.0634	0.7336
15 SLF_THINCRUST	0.0037	-0.0417	-0.1947	0.0169	-0.0085	-0.0374	-0.1969	0.2553
16 SLF_THICKCRUST	-0.0739	-0.2015	-0.2061	0.0069	-0.0587	-0.2221	-0.2230	0.9648
17 SLF_BOTTOMCRUST	-0.0617	-0.0900	0.0327	-0.0172	-0.0932	-0.1298	0.0343	1.0307
18 BOTTOMCRUST	-0.0697	-0.1418	-0.2649	0.0090	-0.0557	-0.1446	-0.2870	0.7291
19 CRUST	-0.0251	-0.0722	-0.2373	0.0154	-0.0156	-0.1078	-0.3071	0.7056

Table 3. *Standard Deviations of Emissivities of Their Differences for the Data of Table 2.* In case of water (row 1) the numbers represent the difference between the emissivities at 8 °C and 0 °C

0	1 $e_h$ 4.9	2 $e_h$ 10.4	3 $e_h$ 21	4 $e_h$ 35	5 $e_h$ 94	6 $e_r$ 4.9	7 $e_r$ 10.4	8 $e_r$ 21
1 WATER_0-8C	0.0010	-0.0057	-0.0166	-0.0258	-0.0391	0.0017	-0.0088	-0.0238
2 BARE_SOIL	0.0740	0.0482	0.0349	0.0339	0.0209	0.0333	0.0293	0.0230
3 FROZEN_SOIL	0.0023	0.0037	0.0093	0.0006	0.0009	0.0048	0.0019	0.0097
4 SLF_BARE	0.0251	0.0232	0.0163	0.0214	0.0380	0.0183	0.0197	0.0168
5 SHORT_GRASS	0.0076	0.0075	0.0114	0.0095	0.0082	0.0115	0.0079	0.0101
6 MEDIUM_GRASS	0.0068	0.0093	0.0108	0.0121	0.0229	0.0014	0.0036	0.0062
7 FROZEN_GRASS	0.0220	0.0078	0.0042	0.0058	0.0093	0.0122	0.0062	0.0044
8 FROST_GRASS	0.0073	0.0058	0.0037	0.0042	0.0078	0.0082	0.0045	0.0038
9 GRASS_AFTER_SNOW	0.0130	0.0133	0.0044	0.0038	0.0063	0.0071	0.0073	0.0020
10 SLF_WET	0.0731	0.0705	0.0533	0.0424	0.0424	0.0212	0.0184	0.0157
11 POWDER	0.0292	0.0216	0.0079	0.0262	0.0226	0.0045	0.0053	0.0097
12 SLF_SHALLOW	0.0201	0.0224	0.0315	0.0533	0.1412	0.0068	0.0052	0.0141
13 SLF_MEDIUM	0.0151	0.0349	0.0626	0.0422	0.0912	0.0059	0.0121	0.0299
14 SLF_DEEP	0.0255	0.0412	0.0476	0.0644	0.1039	0.0107	0.0116	0.0353
15 SLF_THINCRUST	0.0535	0.0312	0.0234	0.0426	0.1360	0.0235	0.0097	0.0084
16 SLF_THICKCRUST	0.0320	0.0223	0.0545	0.1023	0.0469	0.0061	0.0049	0.0369
17 SLF_BOTTOMCRUST	0.0091	0.0131	0.0122	0.0493	0.0837	0.0038	0.0079	0.0114
18 BOTTOMCRUST	0.0098	0.0176	0.0799	0.0970	0.0151	0.0043	0.0017	0.0417

0	9 $e_r$ 35	10 $e_r$ 94	11 $v-h$ 4.9	12 $v-h$ 10.4	13 $v-h$ 21	14 $v-h$ 35	15 $v-h$ 94	16 $h10-h5$
1 WATER_0-8C	-0.0333	-0.0354	0.0007	-0.0031	-0.0072	-0.0075	0.0037	-0.0067
2 BARE_SOIL	0.0242	0.0135	0.0413	0.0193	0.0119	0.0109	0.0076	0.0373
3 FROZEN_SOIL	0.0007	0.0014	0.0071	0.0018	0.0004	0.0013	0.0005	0.0014
4 SLF_BARE	0.0194	0.0394	0.0109	0.0104	0.0132	0.0085	0.0017	0.0203
5 SHORT_GRASS	0.0083	0.0097	0.0055	0.0026	0.0032	0.0034	0.0049	0.0030
6 MEDIUM_GRASS	0.0076	0.0163	0.0057	0.0074	0.0081	0.0083	0.0092	0.0069
7 FROZEN_GRASS	0.0042	0.0076	0.0149	0.0037	0.0015	0.0038	0.0037	0.0149
8 FROST_GRASS	0.0011	0.0065	0.0089	0.0015	0.0005	0.0047	0.0014	0.0043
9 GRASS_AFTER_SNOW	0.0017	0.0049	0.0059	0.0060	0.0064	0.0055	0.0013	0.0003
10 SLF_WET	0.0150	0.0357	0.0603	0.0603	0.0418	0.0354	0.0215	0.0625
11 POWDER	0.0109	0.0124	0.0248	0.0178	0.0131	0.0154	0.0133	0.0259
12 SLF_SHALLOW	0.0479	0.1480	0.0161	0.0182	0.0208	0.0149	0.0280	0.0207
13 SLF_MEDIUM	0.0428	0.1047	0.0149	0.0272	0.0506	0.0430	0.0194	0.0239
14 SLF_DEEP	0.0636	0.1113	0.0210	0.0327	0.0222	0.0201	0.0285	0.0332
15 SLF_THINCRUST	0.0386	0.1400	0.0442	0.0253	0.0198	0.0150	0.0261	0.0605
16 SLF_THICKCRUST	0.1043	0.0692	0.0307	0.0218	0.0293	0.0107	0.0279	0.0422
17 SLF_BOTTOMCRUST	0.0345	0.0723	0.0086	0.0159	0.0083	0.0214	0.0214	0.0099
18 BOTTOMCRUST	0.0876	0.0020	0.0056	0.0159	0.0381	0.0094	0.0132	0.0078

0	17 $h21-h10$	18 $h35-h21$	19 $h94-h35$	20 $v10-v5$	21 $v21-v10$	21 $v35-v21$	23 $v94-v35$	24 COMB
1 WATER_0-8C	-0.0109	-0.0092	-0.0133	-0.0104	-0.0150	-0.0095	-0.0021	0.0558
2 BARE_SOIL	0.0166	0.0149	0.0150	0.0112	0.0100	0.0099	0.0124	0.0296
3 FROZEN_SOIL	0.0056	0.0087	0.0003	0.0067	0.0078	0.0104	0.0021	0.0052
4 SLF_BARE	0.0111	0.0136	0.0078	0.0119	0.0079	0.0086	0.0112	0.0440
5 SHORT_GRASS	0.0078	0.0036	0.0066	0.0060	0.0050	0.0030	0.0083	0.0153
6 MEDIUM_GRASS	0.0043	0.0026	0.0149	0.0030	0.0038	0.0020	0.0091	0.0270
7 FROZEN_GRASS	0.0069	0.0041	0.0071	0.0064	0.0029	0.0019	0.0071	0.0142
8 FROST_GRASS	0.0026	0.0074	0.0044	0.0045	0.0027	0.0029	0.0073	0.0118
9 GRASS_AFTER_SNOW	0.0090	0.0006	0.0025	0.0002	0.0093	0.0003	0.0066	0.0091
10 SLF_WET	0.0455	0.0299	0.0632	0.0148	0.0084	0.0126	0.0344	0.1124
11 POWDER	0.0268	0.0197	0.0372	0.0032	0.0044	0.0180	0.0205	0.0601
12 SLF_SHALLOW	0.0292	0.0395	0.1413	0.0066	0.0130	0.0410	0.1310	0.1621
13 SLF_MEDIUM	0.0324	0.0398	0.0759	0.0105	0.0201	0.0304	0.1049	0.1234
14 SLF_DEEP	0.0339	0.0368	0.1201	0.0107	0.0265	0.0369	0.1342	0.1934
15 SLF_THINCRUST	0.0395	0.0344	0.1112	0.0176	0.0101	0.0328	0.1112	0.1341
16 SLF_THICKCRUST	0.0449	0.0588	0.1088	0.0046	0.0355	0.0701	0.1131	0.3307
17 SLF_BOTTOMCRUST	0.0155	0.0510	0.0441	0.0046	0.0051	0.0390	0.0456	0.1344
18 BOTTOMCRUST	0.0622	0.0171	0.1121	0.0025	0.0400	0.0458	0.0895	0.3209

0–1 cm soil layer, respectively (Mätzler, 1992a). The rocky soil of Weissfluhjoch (Fig. 1c) shows a similar average behaviour, but has smaller standard deviations, because the water content cannot change strongly on the rocky surface. The frozen bare soil (Fig. 1b), however, shows high and almost constant emissivities due to the low dielectric permittivity.

All grass emissivities look very similar. Three of the five classes are represented by Figs. 1d, e and f. At high frequencies short grass (Fig. 1d) shows slightly higher emissivities than medium grass (Fig. 1e), but the opposite is true at low frequencies. There the more reflective soil is better visible for short grass. On the other hand, the slightly lower emissivities of medium grass above 20 GHz result from increased volume scattering on the longer and bending stalks and leaves. This effect is even more pronounced in covers of high grass in summer (Mätzler, 1992a). In case of Fig. 1f (grass with hoar-frost) the emissivity is slightly depressed at both the highest and the lowest frequency. At 5 GHz the transparency of the grass canopy is increased due to the frozen state, and the soil emissivity is apparent whereas at 94 GHz the volume scattering of the surface hoar influences the emissivity. In the case of frozen grass without surface-hoar crystals the 94 GHz values are higher with the remaining emissivities being almost the same as those of Fig. 1f. A special case is the grass after snowmelt (all snow is gone) where all emissivities are depressed to values near 0.90.

The remaining Figs. 1g to 1o show spectra of different types of snow, completely dry snow without melt metamorphism in Figs. 1g, h, i and j, wet snow in Fig. 1k, and refrozen crusts in Figs. 1l to 1o.

Dry snow and refrozen crusts are characterized by low emissivities at high frequencies; for powder snow this is true only at 94 GHz (Fig. 1g). In addition, the winter snow is also characterized by relatively high polarization differences, especially at the intermediate frequencies (10 to 35 GHz). There is no significant difference between the average spectra of shallow, medium and deep winter snow. Dramatic variations exist at 94 GHz within the same range in all three classes; on the other hand, low standard deviations exist at 5 and 10 GHz for  $e_v$ . A closer look shows that with increasing snow water equivalent, the polarization

difference increases, especially at 5 to 10 GHz. This will be discussed later.

The spectra of wet snow (Fig. 1k) are clearly different from those of dry snow. There is an apparent similarity with bare soil (Fig. 1a). Wet snow, however, shows a flat maximum at about 20 GHz, whereas for bare soil the emissivity increases with frequency up to 94 GHz. The decrease of  $e_v - e_h$  with increasing frequency is slower in case of wet snow.

Figures 1l and 1m show the spectra of the classes, thin crust and thick crust, both on top of wet snow of the test site, Weissfluhjoch, and Fig. 1o gives the spectra of crusts frozen to the ground (bottom crust) at the test site in Moosseedorf. These spectra are characterized by low polarization differences and by a Rayleigh spectrum (proportional to  $f^4$ ) of the reflectivity (Mätzler, 1987; Reber et al., 1987) due to the dominant scattering on the large, quasi-spherical snow grains of the refrozen crusts. Here the volume scattering is limited to the dry surface layer, and the wet snow acts as a black-body background, especially at vertical polarization. Indeed we find the highest emissivities for  $e_v$  at 5 and 10 GHz in Fig. 1m with extremely small variability. At these frequencies the Rayleigh scattering of the crust is very small. At  $e_h$  it is sometimes possible to observe an interference effect between the small reflections at the surface and at the interface between the dry and wet snow (Mätzler, 1987; Fig. 4.26). On the other hand the large standard deviation found at 35 and 94 GHz is related to the systematic increase of volume scattering with increasing crust thickness.

The low polarization difference is typical for crusts which had been wet before for many days which allowed the layered snow structure to be disintegrated into the isotropic, granular medium of old, wet snow. For crusts that occur early in the melt season or during short, warm periods in winter, the polarization difference tends to be larger. Examples are given in Tables 2 and 3 by the object classes SLF\_BOTTOMCRUST of Weissfluhjoch (Fig. 1n) and CRUST of Moosseedorf. Finally, the BOTTOMCRUST of Moosseedorf again shows a similar spectrum (Fig. 1o) as the thick crust (Fig. 1m). However, the emissivities at 5 and 10 GHz are clearly lower. The reason is the missing layer of wet snow below the

crust, i.e. we see significant scattering at the ground surface.

### 2.5 Complementary Information on Emissivities

Besides the object classes described above, we need emissivity information of further winter landscapes. Most important are lakes (frozen and unfrozen), swamps or boglands and forests.

- (a) The emissivities of calm, unfrozen lakes can well be represented by computed values based on the Fresnel formula with the results shown in Row 1 of Tables 2 and 3. The low emissivities at low microwave frequencies are a sharp contrast to the other data. Also the large polarization differences are characteristic signatures of water surfaces.
- (b) When lakes freeze, their emissivity increases. Multifrequency observations of a freshwater lake in Colorado made by Hall et al. (1981) showed a linear relationship between ice thickness and brightness temperature at 5 GHz over a thickness range from 20 to 70 cm. At the higher frequencies (22 and 37 GHz) the microwave radiation was dominated by the snow properties. When the snow gets wet the penetration depth is reduced drastically to about one wavelength (Ulaby et al., 1981); then any snowcover on the ice will dominate and emit radiation like wet snow on land. We should also mention that small amounts of salts and other ionic impurities in lake water increase the dielectric loss of lake ice (Mätzler and Wegmüller, 1987; Errata, 1988). Therefore we need more experimental data.
- (c) For boglands we have no in-situ measurements. However, SMMR-data analysis has shown that bogland emissivities are similar to those of farmlands (Tiuri and Hallikainen, 1981; Hallikainen, 1984).
- (d) Spectral emissivities of forest elements such as small trees, twigs and leaves were measured at the PAMIR frequency range by Sume et al. (1988), and by Wegmüller et al. (1993). These data indicate high emissivities for coniferous trees and lower emissivities at the higher PAMIR frequencies for trees with broad leaves. Orientational effects are important. Trees with a pronounced horizontal orientation of the leaves show low emissivities. These results were confirmed by actual forest measurements

with an imaging 90 GHz radiometer flown on aircraft (Süss et al., 1989). Coniferous trees showed a near black-body behaviour, and foliated broad-leaf trees showed reduced brightness temperatures by about 20 K.

In winter, the broad leaves are missing, and since branches and twigs are rather vertically oriented, we expect higher emissivities and thus similar values for all forest types. Snowcovers in forests have higher emissivities than snowcovers in un-forested areas due to the interaction with the trees (Hallikainen, 1984). Dedicated experiments to study this interaction should be carried out. It was found that the transmissivity of microwaves at all PAMIR frequencies through twigs of conifers is highly sensitive to temperature (Wegmüller et al., 1993; Mätzler and Wegmüller, 1993).

## 3. Spectral Signatures for Classification

### 3.1 Signatures for Snow Mapping

The ideal situation for snow mapping is found when all snow types have the same brightness, when all snow-free objects look the same, and when the contrast between snow and snow-free state is large. In this ideal case, snow has "on-off" signature. It can be used to delineate the snow boundary and also to determine snow coverage in mixed-signature situations.

At passive microwaves, the situation is not ideal. Nevertheless, all snow types with a dry surface show the common signature of volume scattering: a negative spectral gradient in the 20 to 100 GHz range with low emissivities at 35 GHz (except for powder snow) and 90 GHz (Table 2). Except for wet snow, the ideal situation is almost met at  $e_v$  (90 GHz). Even water has a higher emissivity. For the following reasons, however, a snow-mapping algorithm should not rely exclusively on the 90 GHz data:

- (1) The atmospheric transparency is variable and it can be quite low (Mätzler, 1992b).
- (2) Only a thin surface layer of the snowcover determines the actual emissivity. For new snow the grain size can be very small leading to higher emissivities than the other types of dry snow at 35 and 90 GHz. The class POWDER snow represents this situation (row 11 of Table 2).
- (3) Precipitating clouds can show low emissivities,

similar to the ones of dry snow (Neale et al., 1990).

Due to these problems the 90 GHz data should only be regarded as complementary.

At lower frequencies the difficulty with wet snow remains. However, the atmospheric transparency is much higher and therefore more stable. Furthermore, the problem with new (powder) snow is reduced due to its high transparency. Another advantage of the lower frequencies is the relatively high polarization difference of several snow types in contrast to snow-free land. Even wet snow has certain signature properties as will be shown below.

The signature properties of Tables 2 and 3 will be illustrated with the following decision – tree algorithm (an analogous procedure is possible on the basis of brightness temperatures):

3.1.1 First, we see from Columns 6 and 7 that  $e_v$  at 5 to 10 GHz is about 0.5 for water surfaces and near 0.9 or higher for all other surfaces. This is the clearest signature for the discrimination of water from all other surface types. Although the contrast is still larger at horizontal polarization (Cols. 1 and 2) the variability, especially of bare soil and of wet snow, hampers the application of horizontal polarization in mixed situations.

3.1.2 Second, after having eliminated water areas, we use the linear combination COMB (Col. 24) to separate snow from snow-free areas. This linear combination is defined as

$$\text{COMB} = e_v(10) - e_h(10) + e_v(21) - e_h(21) + e_v(35) - e_h(35) + 3[e_v(10) - e_v(35)]. \quad (2)$$

COMB is an optimum balance between polarization and spectral gradient in such a way that all snow-free types (except water) have values between 0.03 and 0.09, and even if the standard deviations of Table 3 are considered we find that COMB is mostly between 0.0 and 0.1. On the other hand, all types of snow show COMB values larger than 0.1, typically 0.7. Only the case of powder snow is marginal with  $\text{COMB} = 0.126 \pm 0.060$ . With the 94 GHz data we are able to discriminate this snow type more clearly. Wet snow is a less serious problem due to its high polarization difference. And in cases where this difference is small (as a result of small liquid water content) there appears

a contribution from the spectral differences as a result of volume scattering.

3.1.3 Third, after having eliminated water and snow-free areas we apply the spectral differences at vertical polarization to discriminate wet from dry snow. Wet snow has values close to 0.0 in Columns 21 to 23, whereas dry snow has large negative values in at least one of these columns. Volume scattering is the physical process behind the dry-snow signature. Horizontal polarization is less suitable due to its higher variability within each class.

If we want to find areas of wet snow below a layer of dry snow there is no direct way for discrimination as long as we accept variable thickness and variable structure of the overlying dry snow. However, one thing common to these situations is their rapid time variation. The discrimination of refrozen crust on top of wet snow is easier due to the small polarization difference combined with large negative values in Column 23, and at the same time high  $e_v$  values in excess of 0.98 at 10 GHz (Column 7).

### 3.2 Signatures of Snow-Free Land Areas

Small COMB values are indicative of snow-free land areas. Within these classes (Rows 2 to 9 of Tables 2 and 3) we may be able to separate bare from vegetated areas. The most evident signature of bare surfaces is the large polarization difference at 5 GHz (Column 11). Another signature is the spectral difference of Column 16; its advantage is its reduced sensitivity of freezing conditions.

On the other hand if we want to identify frost in areas with bare soil, we should look for high  $e_h$  values at 5 or at 10 GHz. However, ambiguities with vegetated areas must be avoided by multi-temporal observations or by a-priori knowledge.

The identification of frost in vegetated areas must be based on the measurement of the surface temperature (Section 4.1).

### 3.3 Incorporation of Mixed Situations

The  $e_v$  signature of water at 10 GHz is so clear that it will be possible to estimate fractions of open water within the footprint of 10 GHz brightness temperature at vertical polarization. Other mixed situations are more difficult to identify. Here one should rely on multi-temporal analysis.

#### 4. Spectral Signatures for Estimation of Physical Parameters

##### 4.1 Estimation of Effective Surface Temperatures

###### 4.1.1 Seasonal Snow

One of the most important parameters is the surface temperature  $T$ . When combined with the emissivity the surface temperature sensed by a radiometer is an effective temperature, a weighted average value over the penetration depth at the given frequency. When the emitting medium is isothermal the effective temperature is equal to the actual surface temperature. This is valid in case of wet snow where  $T = 273.2$  K. Then we know the temperature already from the result of object classification. The same is true for thin and thick crusts overlying wet snow where the effective temperature is equal to the temperature at the interface between dry and wet snow (with the exception of data at 94 GHz). In case of dry winter snow or of bottom crusts the microwaves usually penetrate through seasonal snowpacks at least at frequencies below 30 GHz (Mätzler, 1987; Rott, 1989). Then the effective temperature is equal to the physical temperature at the base of the snow-cover. In most regions with seasonal snow this temperature is close to or a few degrees below the

freezing point of water. Therefore, surface-temperature retrievals in areas of seasonal snowpacks are either indirect through snow classification or impossible due to the deep sensing.

###### 4.1.2 Snow-Free Land Areas

On snow-free land the microwave penetration is usually quite small. The effective temperature is the canopy temperature in cases with a vegetation cover or the soil temperature at the depth of a fraction of a wavelength in cases of bare soil. Even frozen soil is quite lossy (Ulaby et al., 1986). Exceptions may occur only under extreme dryness. If the emissivity is high the emitted brightness temperature is close to the effective temperature. At low frequencies (5 to 10 GHz) the atmospheric effect is so small that we can neglect it. If we neglect also the cosmic background radiation, then  $T_p$  ( $p = v, h$ ) is simply proportional to  $e_p$  and  $T$ ,

$$T_p = e_p T. \quad (3)$$

By using a suitable linear combination of  $T_p$  values from the same area we can reduce the uncertainty of  $e_p$ . As an example, Table 4 shows values of  $e_x$ , defined by

$$e_x = 2e_v - e_h \quad (4)$$

Table 4. Values of  $e_x$  as Defined by Eq. (4) for all Object Classes at the PAMIR Frequencies

0 Object	1 $2e_v - e_h$ 4.9	2 $2e_v - e_h$ 10.4	3 $2e_v - e_h$ 21	4 $2e_v - e_h$ 35	5 $2e_v - e_h$ 94
1 WATER_0-8C	0.7514	0.7881	0.8681	0.9541	1.1269
2 BARE_SOIL	1.0226	0.9584	0.9321	0.9235	0.9521
3 FROZEN_SOIL	0.9886	0.9628	0.9644	0.9526	0.9618
4 SLF_BARE	1.0020	0.9854	0.9710	0.9727	0.9602
5 SHORT_GRASS	0.9506	0.9621	0.9379	0.9281	0.9529
6 MEDIUM_GRASS	0.9700	0.9624	0.9394	0.9357	0.9533
7 FROZEN_GRASS	0.9802	0.9730	0.9530	0.9494	0.9591
8 FROST_GRASS	0.9776	0.9736	0.9536	0.9474	0.9461
9 GRASS_AFTER_SNOW	0.9224	0.9387	0.9089	0.9178	0.9347
10 SLF_WET	1.0968	1.0773	1.0407	1.0220	0.9730
11 POWDER	0.9962	0.9901	0.9805	0.9765	0.8921
12 SLF_SHALLOW	1.0027	1.0299	1.0095	0.9284	0.7048
13 SLF_MEDIUM	1.0228	1.0445	1.0145	0.8878	0.7254
14 SLF_DEEP	1.0440	1.0753	1.0165	0.9113	0.8021
15 SLF_THINCRUST	1.0334	1.0302	1.0096	0.9766	0.7802
16 SLF_THICKCRUST	1.0561	1.0273	0.9838	0.7411	0.5114
17 SLF_BOTTOMCRUST	1.0565	1.0768	0.9522	0.7825	0.8185
18 BOTTOMCRUST	1.0073	0.9879	0.9462	0.7989	0.4896
19 CRUST	1.0094	1.0502	1.0441	0.9007	0.5237

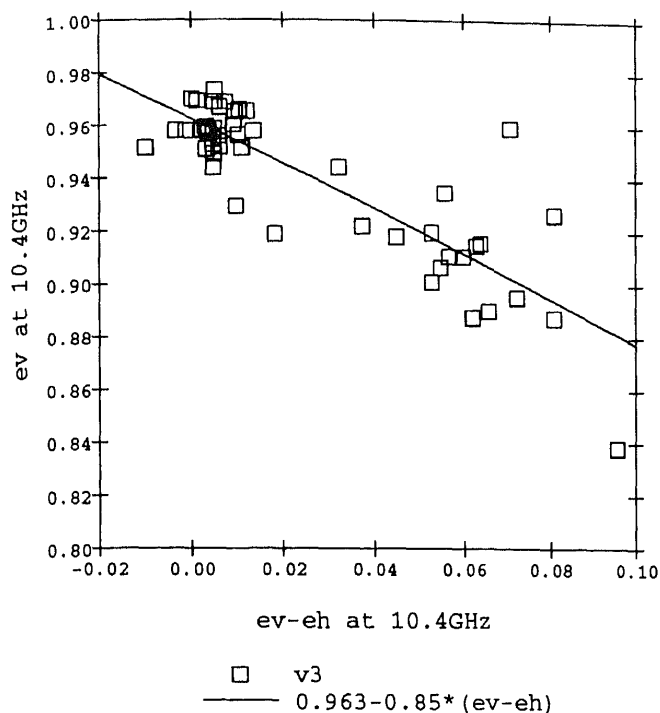


Fig. 2. Vertically polarized emissivity  $e_v$  at 10.4 GHz versus the difference  $e_v - e_h$  at 10.4 GHz of all 47 snow-free winter land surfaces measured by PAMIR

of all object classes at all PAMIR frequencies. These  $e_x$  values are quite stable. The idea for selecting the special linear combinations  $e_x$  according to Eq. (4) came from scatterplots of  $e_v$  versus the polarization difference  $e_v - e_h$ . The example of the snow-free land data is shown in Fig. 2 together with a linear least-squares fit. For the snow-free land data (excluding water) the 10.4 GHz data of  $e_x$  are near 0.966 with a standard deviation of 0.017. If we accept this variability as our uncertainty of  $e_x$  we can estimate  $T$  from

$$T = (2T_v - T_h)/0.966 \quad (5)$$

with an uncertainty of less than 5 K at  $T < 290$  K. Also at the other frequencies we find quite stable  $e_x$  values.

The fact that even water surfaces and snow show  $e_x$  values close to 1.0 makes Eq. (5) insensitive to small cover fractions of lakes or snow within the footprint. Only at 94 GHz can we find exceptionally small  $e_x$  values.

#### 4.2 Estimation of the Liquid Water Content of Snow Surfaces

The measurement of soil moisture by microwave radiometry is well known (e.g. Jackson and Schmugge, 1989) and does not have to be repeated

here. It is based on the increase of the surface reflectivity with increasing liquid water content. The same physical mechanism also holds for the estimation of snow liquid water. Main differences of the snow properties as compared to soil are (1) smaller dielectric permittivities due to the lower content of liquid water, and (2) less variation of the surface roughness. In addition, since snowpacks usually cover the vegetation, there are less problems of screening by vegetation, allowing frequencies above  $L$ -band to be used. Snow wetness at the surface of the snowpack can be determined from brightness temperatures at horizontal polarization (Mätzler et al., 1984; Mätzler, 1987). As will be shown below the relation between the volumetric liquid water content,  $W$ , and the reflectivity,  $r_h$  (Eq. 1), is a linear function in the range  $0 < W < 15\%$ , being the typical range of snow wetness.

The relation between  $r_h$  and  $W$  is based (a) on the observation (Figs. 2.24–2.25 of Mätzler, 1987) that for wet snow  $r_h$  can be approximated by the Fresnel formula over a wide frequency range (Exceptions occur when the vertical inhomogeneity at the surface is strong), and (b) on the complex dielectric permittivity,  $\epsilon$ , which is a function of frequency,  $f$ , density,  $\rho$ , and liquid water content,  $W$ :

$$\epsilon = \epsilon_\infty + \frac{\epsilon_s - \epsilon_\infty}{1 - if/f_0} \quad (6)$$

where the relaxation frequency  $f_0 = 10$  GHz for wet snow, and  $i$  is the square root of  $-1$ . The two parameters  $\epsilon_\infty$  and  $\epsilon_s$  are given by

$$\epsilon_\infty = 1 + \frac{1.60\rho}{1 - 0.35\rho}, \quad \epsilon_s = \epsilon_\infty + 0.187W + 0.0045W^2 \quad (7)$$

where  $W$  is in (%) and  $\rho$  is the snow density in  $\text{g/cm}^3$ . The equation for  $\epsilon_\infty$  is identical to the density dependence of the dielectric permittivity of dry snow (Mätzler, 1987), and the equation for  $\epsilon_s$  was given by Denoth (1989).

From (1), (6) and (7), and the Fresnel formula for  $r_h$  we obtain the functional dependence  $r_h(f, W, \rho, \theta)$  at the incidence angle  $\theta$ . Results are plotted in Fig. 3 for  $\theta = 50^\circ$ ,  $f = 6.8$  GHz,  $\epsilon_\infty = 1.6$ , 1.8 and 2.0, respectively, corresponding to snow densities of 0.332, 0.425 and 0.512  $\text{g/cm}^3$  (Eq. 7). This is a typical range for wet snow. At the MIMR

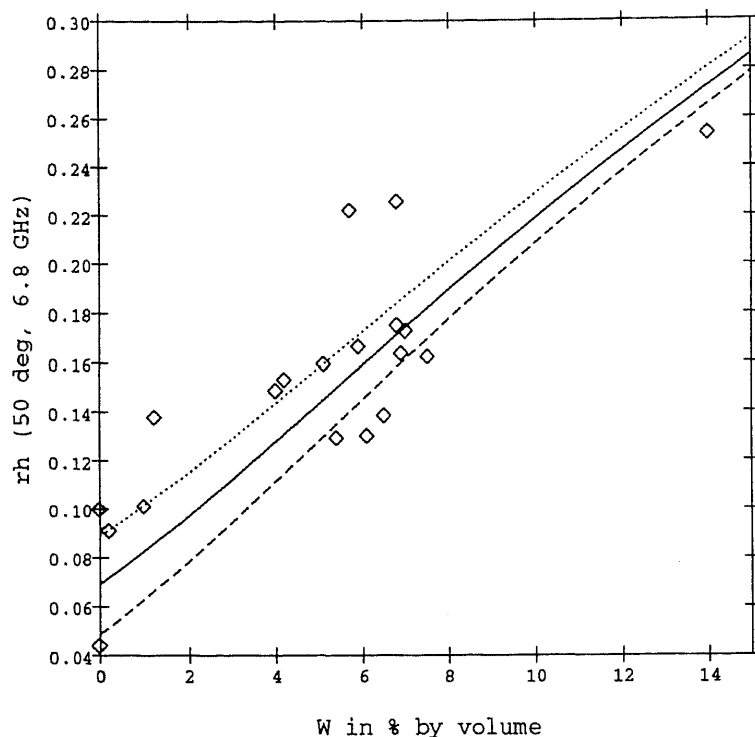


Fig. 3. Reflectivity  $r_h$  at  $f = 6.8$  GHz,  $50^\circ$  of incidence versus liquid water content  $W$ . The curves show computed values of  $r_h$  for 3 values of  $\epsilon_\infty$ : 1.6 (bottom curve, dashed), 1.8 (solid line), 2.0 (top curve, dotted). Diamonds are measured data

frequency, 6.8 GHz, the curves are extremely close to linear within the  $0 < W < 15\%$  range. At higher frequencies, a more and more non-linear behaviour is found with a decreasing sensitivity to  $W$ . Also shown in Fig. 3 are measured data; they were extracted from Mätzler et al. (1984) and Mätzler and Sume (1986). The  $r_h$  values at 6.8 GHz were interpolated from PAMIR data at 4.9 GHz and 10.4 GHz, and the  $W$  values were determined from dielectric measurements made in the 1 GHz range at the 0–2 cm surface layer. The extreme data point at  $W = 14\%$  resulted from a situation with rain. The comparison of Fig. 3 is satisfactory, because when considering the scatter of the data points around the computed lines it should be kept in mind that snow wetness is laterally heterogeneous at the decimeter scale due to the formation of drainage channels. The dielectric point measurements are subject to this heterogeneity and therefore scatter strongly. On the other hand the radiometer footprint covered several  $m^2$ , thus averaging took place over the heterogeneity.

For old, wet snow the density is often close to  $0.4 \text{ g/cm}^3$ . Then for a given frequency and incidence angle the only variable of  $r_h$  is the liquid water content  $W$ . Using the relationship shown in Fig. 3 for  $f = 6.8$  GHz together with Eq. (1) (where  $T = 273.2 \text{ K}$  and  $T_s \approx 8 \text{ K}$ ) we can derive a linear relationship between  $T_h$  and  $W$ . With the help of

the Fresnel equation and Eqs. (1), (6) and (7), the algorithm can be adapted to other microwave frequencies up to about 20 GHz.

#### 4.3 Estimation of the Water Equivalent of Dry Snow

Although the Water Equivalent WE is the most important snowpack parameter from the hydrologic point of view and although microwave radiation at  $f < 40$  GHz can easily penetrate through typical packs of dry, seasonal snow, the estimation of WE by microwave radiometry is not at all an easy task. This was realized already by Mätzler et al. (1982) on the basis of the early Weissfluhjoch data, by Wang et al. (1992) with aircraft data over Alaska, and also by Künzi et al. (1982) and by Hallikainen and Jolma (1986) on the basis of SMMR data.

The problem with satellite data is certainly related to the fact that within one footprint of the sensor the snowpack is a composition of different snowtypes and of snow-free areas. But even if we reduce the problem to the in-situ measured observable of dry winter snow (POWDER, SLF\_SHALLOW, SLF\_MEDIUM, SLF\_DEEP) an accurate inversion algorithm does not exist. (With the inclusion of crusts and wet snow the situation would become even more ambiguous).

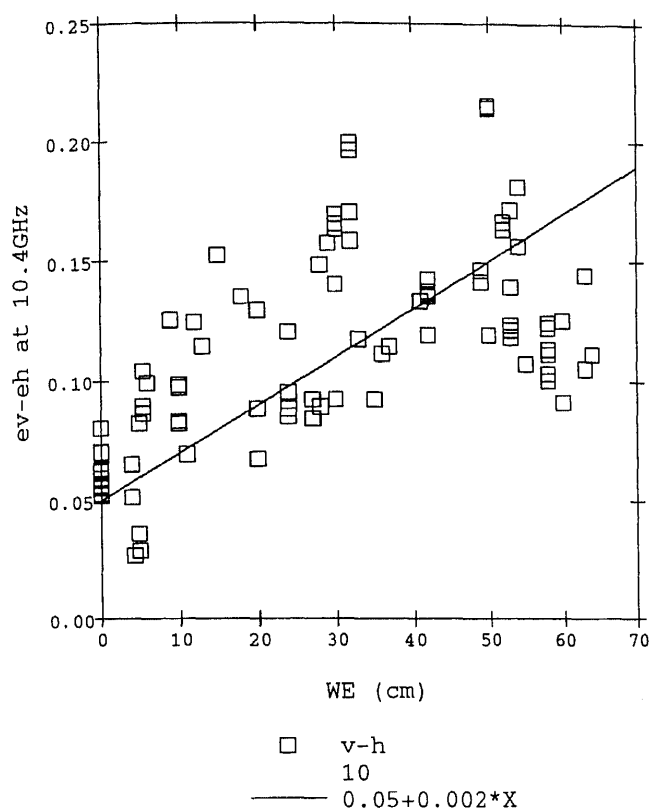


Fig. 4. Polarization difference  $e_v - e_h$  of winter snow at 10.4 GHz versus WE together with a linear fit

We will describe the situation with scatterplots showing these winter data versus WE together with the snow-free data of Weissfluhjoch as a reference for  $WE = 0$ . Figure 4 shows the polarization difference at 10.4 GHz. With increasing WE this difference tends to increase up to the largest WE values.

At higher frequencies the signal is more sensitive to the presence of snow. Figure 5 shows  $e_v$  and  $e_h$  at 35 GHz versus WE, and Fig. 6 shows COMB values (2) versus WE. For WE values increasing from 0 to 10 cm both Figs. 5 and 6 show a rapid change of their dependent variables. However, for larger water equivalents the behaviour of the data changes and their values scatter over a larger range. The  $e_v$  values of Fig. 5 even tend to increase up to 0.9 for the deepest snowpacks making it difficult to discriminate such situations from snow-free surfaces. This problem is less serious in Fig. 6.

The physical reason for the shown behaviour is the strong dependence of the emissivities at high microwave frequencies on the grain size of the snowpack. For Rayleigh scattering the emissivity decreases proportional to the third power of the

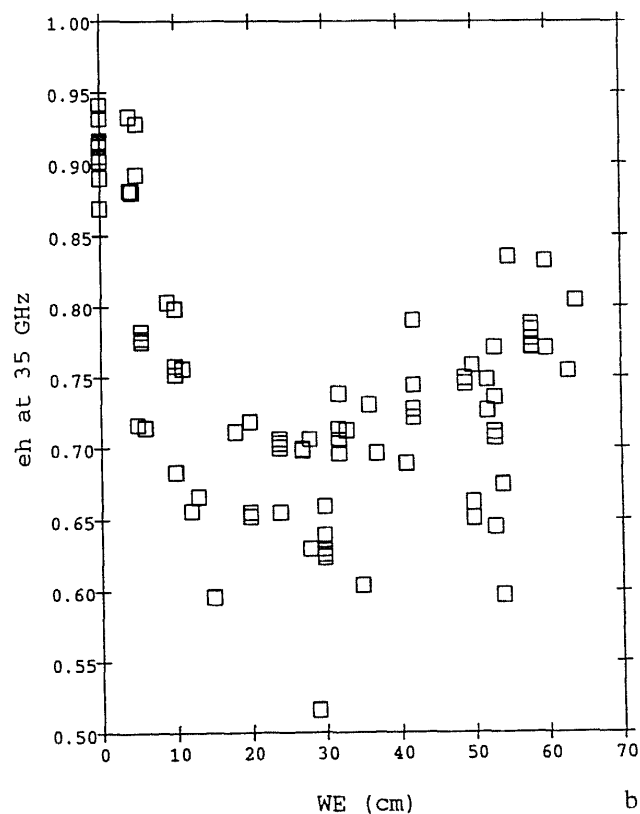
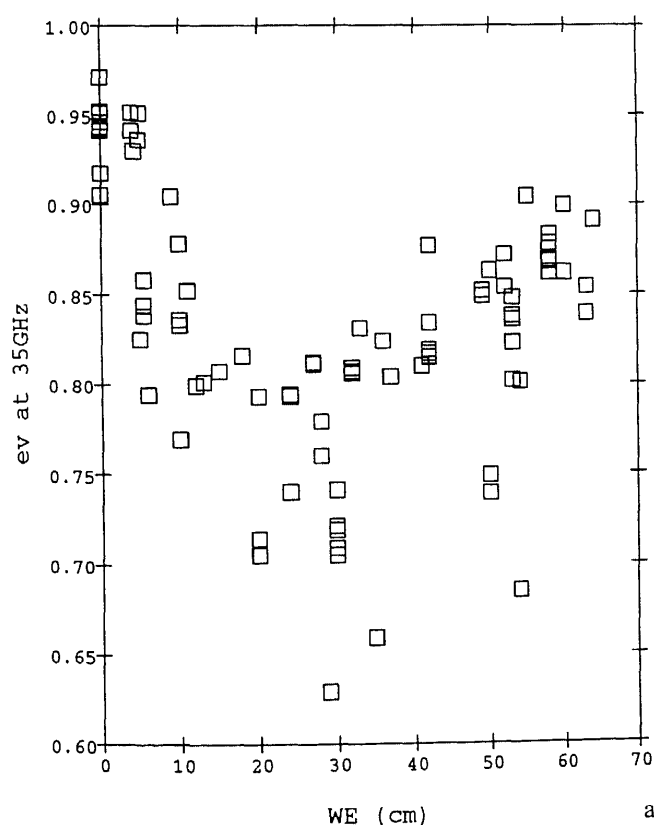


Fig. 5. Emissivities at 35 GHz of winter snow versus WE: (a) vertical, (b) horizontal polarization

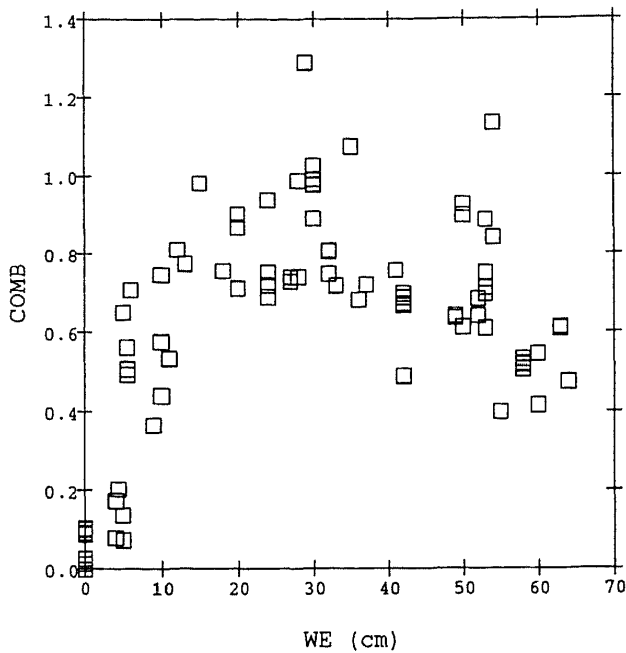


Fig. 6. Linear combination (Eq. 2) of emissivities of winter-snow data versus WE

grain radius, assuming WE to be constant (Mätzler, 1987). This is also true for non-spherical grains where the sensitive grain size is the smallest dimension of the grain. This quantity not only changes within the snowpack, but it changes also with time. It is mainly the temperature-gradient metamorphism which makes snow grains grow near the bottom of winter snowpacks (Colbeck, 1982). For shallow snowpacks the temperature gradient tends to be large, the production of large grains of depth hoar is efficient and fast. This explains the low emissivities at WE values near 20 cm (Fig. 5). On the other hand for deep snowpacks ( $WE > 25$  cm, SLF\_DEEP) the temperature gradient is weaker with the result that less depth hoar is formed. Then the snow remains fine-grained, and the emissivity remains high.

The monotonous trend found in Fig. 4 is related to layering and not to grain size. The deeper the pack the more layers are to be expected. The polarization-dependent reflection at each layer interface increases the polarization difference,  $e_v - e_h$ , with increasing depth.

The estimation of the water equivalent on the basis of Figs. 4 to 6 is very inaccurate. It is possible, however, that the variability of the observables is reduced if the data are averaged over large areas. This averaging will be different in different regions. Therefore we must expect the need for regionalized parameters possibly with seasonal and annual

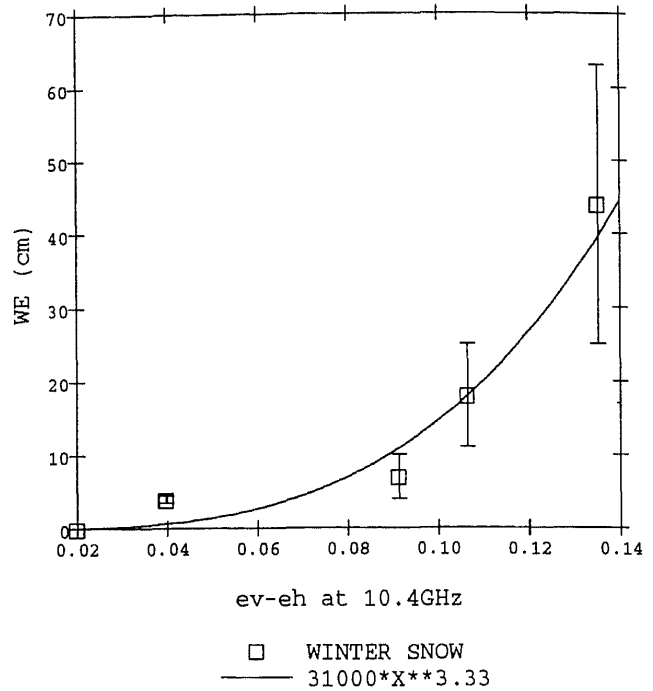


Fig. 7. The WE ranges of object classes, average snow-free areas, powder snow, shallow, medium and deep winter snow, versus average polarization differences,  $e_v - e_h$ , at 10.4 GHz. The curve represents the non-linear fit of Eq. (8)

peculiarities. The possible behaviour of averaged data is illustrated by the average emissivities of Table 2. As an example let us look at the polarization difference at 10.4 GHz for an average snow-free region and for dry winter snow (Rows 11 to 14). If we plot the WE range of these classes versus their polarization difference we get Fig. 7. With the non-linear interpolation

$$WE \text{ (cm)} = 31,000 (e_v - e_h)^{3.33} \quad (8)$$

we obtain an algorithm for estimating WE. This special form should not be regarded as a final result, but rather as an example for a certain observable.

A disturbing effect for the WE algorithms occurs if wet snow or refrozen crusts are present within the scene. In order to reduce their influence we should look for an optimum combination of polarization and spectral-gradient information.

An alternative way for estimating WE could be found through multitemporal analysis using day and night observations throughout the snow season. This will be a topic for further research.

## 5. Conclusions

The systematic composition of spectral emissivities (Table 2) and of their variabilities (Table 3) of

object classes of winter landscapes gave a new insight into the radiative signatures of passive microwave sensors over the frequency range from 5 to 100 GHz. The discussion of these properties helped to define criteria for discriminating surface types and snowcover types from multichannel radiometer data. Open water can be discriminated from other surfaces by its low emissivity, e.g. at 10 GHz. Snow-free areas can then be identified by low values of a special combination (COMB) of emissivities. The remaining surfaces of snow can be classified in various types. Problematic is new powder snow. Algorithms were given to estimate physical surface properties such as surface temperature, surface liquid-water content of snow-packs, and tentative algorithms were proposed to estimate the water equivalent of dry winter snow. The discussion was based on emissivity data. Atmospheric effects were not directly considered. However, by emphasizing the importance of data in the 5 to 21 GHz range, the atmospheric effects over winter landscapes are small (Mätzler, 1992b).

In future the data of Tables 2 and 3 should be completed by additional object classes to improve the validity of the proposed algorithms or to find additional criteria. The described long-term effort of microwave signature research should be continued and complemented by new radiometer systems. The advantages of in-situ experiments are the excellent control of ground-truth data and the monitoring capability of temporal changes.

An additional requirement for constructing physical algorithms of remote sensing data is a knowledge of the spatial variability of radiances in question. According to the principle of ergodicity we can expect that at least certain temporal variations are also representative of spatial variations. Nevertheless, for the accurate assessment of algorithms from spatially integrated data we need observations from aircraft to describe the actual spatial heterogeneity of the spectral microwave emissivity. The combination of both types of experiments are necessary. They will lead to the most accurate interpretation of microwave remote sensing data.

#### Acknowledgements

The author likes to thank Erwin Schanda, Head of the Microwave Department at the Institute of Applied Physics, for his continuing interest in and motivation for the microwave

signature studies reported here. Also the questions posed, corrections made and comments given by two anonymous referees are gratefully acknowledged.

#### References

- Armand, N. A., Kutuza, B. G., 1993: Complex of Remote Sensing of the Earth, Priroda, Scientific Program, Version 2, Inst. Radio Eng. Mokhovaija st. 11, Moscow, GSP-3, 103907 Russia.
- Colbeck, S. C., 1982: An overview of seasonal snow metamorphism. *Rev. Geophys. Space Sci.*, **20**, 45–61.
- Denoth, A., 1989: Snow dielectric measurements. *Adv. Space Res.*, **9**, 1, (1)233–(1)243.
- Gloersen, P., Cavalieri, D. J., Change, A. T. C., Wilheit, T. T., Campbell, W. J., Johannessen, O. M., Katsaros, K. B., Künzi, K. F., Ross, D. B., Staelin, D., Windsor, E. P. L., Barath, R. T., Gudmansen, P., Langham, E., Ramseier, R. O., 1984: A summary of results from the first Nimbus-7 SMMR observations. *J. Geophys. Res.*, **89**(D4), 5335–5344.
- Gloersen, P., Campbell, W. J., 1991: Recent variations in Arctic and Antarctic sea-ice covers. *Nature*, **352**, 33–36.
- Hall, D. K., Foster, J. L., Chang, A. T. C., Rango, A., 1981: Freshwater ice thickness observations using passive microwave sensors. *IEEE Trans. Geosci. and Remote Sensing*, **GE-19**, 189–192.
- Hallikainen, M., 1984: Retrieval of snow water equivalent from Nimbus-7 SMMR data: effect of land-cover categories and weather conditions. *IEEE J. Oceanic Engin.*, **OE-9**, 372–376.
- Hallikainen, M. T., Jolma, P. A., 1986: Retrieval of the water equivalent of snow cover in Finland by satellite microwave radiometry. *IEEE Trans. Geosci. and Remote Sensing*, **GE-24**, 855–862.
- Hollinger, J. P., 1990: Editor of special issue on SSMI. *IEEE Trans. Geoscience and Remote Sensing*, **28**, (5), 779–845.
- Jackson, T. J., Schmugge, T. J., 1989: Passive microwave remote sensing for soil moisture: some supporting research. *IEEE Trans. Geosci. and Remote Sensing*, **27**, 225–235.
- Künzi, K. F., Patil, S., Rott, H., 1982: Snow-cover parameters retrieved from Nimbus-7 SMMR data. *IEEE Trans. Geosci. and Remote Sensing*, **GE-20**, 452–467.
- Mätzler, C., Schanda, E., Good, W., 1982: Towards the definition of optimum sensor specifications for microwave remote sensing of snow. *IEEE Trans. Geosci. and Remote Sensing*, **GE-20**, 57–66.
- Mätzler, C., Aebischer, H., Schanda, E., 1984: Microwave dielectric properties of surface snow. *IEEE J. Oceanic Engin.*, **OE-9**, 366–371.
- Mätzler, C., Sume, A., 1986: Microwave measurements of snow in Davos, May–June 1986. *Forsvarets Forskningsansalt (FOA)*, Rapport C30437-3.2, Linköping, Sweden, December 1986.
- Mätzler, C., Wegmüller, U., 1987: Dielectric properties of fresh-water ice at microwave frequencies. *J. Phys. D: Appl. Phys.*, **20**, 1623–1630; Errata (1988), **21**, 1660.
- Mätzler, C., 1987: Application of the interaction of microwaves with the natural cover. *Remote Sensing Rev.*, **2**, 259–392.

- Mätzler, C., 1990: Seasonal evolution of microwave radiation from an oat field. *Remote Sensing Environ.*, **31**, 161–173.
- Mätzler, C., 1992a: Passive microwave signature catalog 1989–1992. *Report of the Institute of Applied Physics*, Bern, December 1992.
- Mätzler, C., 1992b: Ground-based observations of atmospheric radiation at 5, 10, 21, 35 and 94 GHz. *Radio Science*, **27**, 403–415.
- Mätzler, C., Wegmüller, U., 1993: Progress in multi-frequency radiometry of natural objects. *Proceedings of ESA-NASA Workshop St. Lary*, France, January 1993.
- Menard, Y., Thornbury, A., 1989: Feasibility study for a Multi-frequency Imaging Microwave Radiometer, Final Report MIMR-RP-020, Marconi Space Systems, Portsmouth, England.
- Neale, C. M. U., McFarland, M. J., Chang, K., 1990: Land-surface-type classification using microwave brightness temperatures from the Special Sensor Microwave/Imager. *IEEE Trans. Geosci. and Remote Sensing*, **28**, (5), 829–838.
- Reber, B., Mätzler, C., Schanda, E., 1987: Microwave signatures of snow crusts-modelling and measurements. *Int. J. Remote Sensing*, **8**, 1649–1665.
- Rott, H., 1989: Multispectral microwave signatures of the antarctic ice sheet. In: Pampaloni, P. (ed.) *Microwave Radiometry and Remote Sens. Appl.* Utrecht: VSP, 89–101.
- Schanda, E., Hofer, R., 1977: Microwave multispectral investigation of snow. *Proc. 11th Internat. Symp. on Remote Sensing of Environment*, 601–607, Ann Arbor, Mi.
- Schanda, E., 1986: *Physical Fundamentals of Remote Sensing*. Berlin, Heidelberg, New York, Tokyo: Springer.
- Sume, A., Mätzler, C., Hüppi, R., Schanda, E., 1988: Microwave radiometer and scatterometer measurements of vegetation. *Forsvarets Forskingsanstalt (FOA) Rapport C30494-3.2*, Linköping, Sweden.
- Süss, H., Grüner, K., Wilson, W. J., 1989: Passive millimeter-wave imaging, a tool for remote sensing. *Alta Frequenza*, **LVIII**(5–6), 457–465.
- Tiuri, M., Hallikainen, M., 1981: Microwave emission characteristics of snow covered earth surfaces measured by the Nimbus-7 satellite. *11th European Microwave Conference*, Amsterdam, September 1981.
- Ulaby, F. T., Moore, R. K., Fung, A. K., 1981, 1982, 1986: Microwave remote sensing, active and passive. *Dedham, Massachusetts: Artech House*, **1**, 1981, **2**, 1982, **3**, 1986.
- Wang, J. R., Chang, A. T. C., Sharma, A. K., 1992: On the estimation of snow depth from microwave radiometric measurements. *IEEE Trans. Geosci. and Remote Sensing*, **30**, 785–792.
- Wegmüller, U., Mätzler, C., Weise, T., 1993: Absorption von Mikrowellen in Nadelbäumen. *Auftragsstudie* zuhanden der PTT, Institute of Applied Physics, University of Bern, March 1993.

Author's address: C. Mätzler, Institute of Applied Physics, University of Bern, Sidlerstrasse 5, CH-3012 Bern, Switzerland.